J|A|C|S
ARTICLES
Published on Web 02/10/2006

Switching-on Superparamagnetism in Mn/CdSe Quantum Dots

Donny Magana, Susanthri C. Perera, Andrew G. Harter, Naresh S. Dalal, and Geoffrey F. Strouse*

Contribution from the Department of Chemistry and Biochemistry, Florida State University, Tallahassee, Florida 32306-4390

Received August 23, 2005; E-mail: strouse@chem.fsu.edu

Abstract: Mn ion doping of CdSe and other semimagnetic quantum dot (QDs) alloys has been an area of active speculation for over a decade. We report evidence of Mn(II) doping of CdSe grown from a cubic single source precursor that is superparamagnetic (SPM) with a blocking temperature of 40 K following thermal annealing. Prior to thermal annealing the 4 nm Mn/CdSe (1% Mn) QDs exhibit mainly paramagnetic behavior between 300 and 2 K, with a weak antiferromagnetic exchange. Following thermal annealing of the sample, high-temperature ferromagnetic exchange is observed in the magnetization data with the onset of an SPM phase at 40 K that exhibits a coercivity of 0.1 T at 2 K. The switching-on of SPM behavior is believed to be linked to ion migration with formation of $(Se-Mn-Se-Mn-Se-Mn)_n$ centers within the nanocrystal that exhibit coupled magnetic moments. Electron paramagnetic resonance (EPR) provides evidence of two distorted T_d Mn core sites, a clustered site (dipolar broadened), and a localized Mn site (hyperfine-split). The ratio of the EPR signature for the dipolar broadened site increases following annealing and shows a hysteretic response around the blocking temperature. These observations suggest that thermal annealing results in enhanced cluster formation explaining the onset of the SPM phase in these nanoscale materials. Evidence of SPM behavior is evident in the field-dependent non-Langevin magnetization with a tangential loss in the ac-magnetic susceptibility and the Mydosh parameter ($\varphi = 0.16$).

Introduction

Quantum confined magnetic materials with predictable size dependent properties, including ion-doped semimagnetic semiconductors and molecular magnets, are one of the holy grails for spin-related applications at the nanoscale.[1−5] While ferromagnetism has been observed for bulk Mn doped CdSe semimagnetic semiconductors, the reason for the observation remains an area of speculation and is attributed to ion clustering within the lattice.[4,6] Efforts on nanocrystalline Mn(II) doped II−VI semimagnetic quantum dots have also produced conflicting findings in their magnetic characterization depending on the nature of preparation, post-treatment such as thermal annealing, and type of quantum dot.[2,5−8] While it was generally accepted that the conflicting results arose from lack of ion doping due to self-annealing leading to loss of the Mn ions for wurtzite CdSe,[2] in a recent paper by Efros et al. the limited Mn doping was attributed to thermodynamic limitations for Mn ions to add to the growing faces of the wurtzite structure of CdSe and not self-annealing.[6] The findings of Efros et al.[6] raise the issue of possible magnetic interactions when dopant ions are incorporated into the nanocrystalline lattice and, more importantly, the importance of Mn−Se−Mn domains in the structure, ion migration to produce the domains, and the resultant magnetization of the materials that might be achievable. The magnitude of ferromagnetic exchange in ion doped semimagnetic semiconductor quantum dots will be dependent on the clustering of ions, the size of the cluster, the site occupation of the ion, the size of the quantum dot, and changes in the nature of the bonding in the host lattice in quantum-confined materials.

This manuscript discusses the emergence of ferromagnetic exchange in 4 nm 1% Mn/CdSe nanocrytals with a wurtzite crystal lattice. Mn(II) ion doping is achieved using a single source precursor route based on a cubic cluster which seeds the growth of the Mn/CdSe quantum dots. These semimagnetic quantum dots transform into wurtzite lattices as the particle grows, leaving the Mn incorporated in the lattice.[6,9−12] Intriguingly, upon thermal annealing of the Mn/CdSe quantum dot a transition of superparamagnetic (SPM) character with a coercive field is observed. The SPM behavior arises from enhanced

(1) Wolf, S. A.; Awschalom, D. D.; Buhrman, R. A.; Daughton, J. M.; von Molnar, S.; Roukes, M. L.; Chtchelkanova, A. Y.; Treger, D. M. *Science* **2001**, *294*, 1488−1495.
(2) Gamelin, D. R. Doped Semiconductor Nanocrystals: Synthesis, Characterization, Physiscal Properties, and Applications. In *Progress in Inorganic Chemistry*; D., K. K., Ed.; John Wiley: New Jersey, 2005; Vol. 54.
(3) Zipse, D.; North, J. M.; Achey, R. M.; Dalal, N. S.; Hill, S.; Edwards, R. S.; Choi, E. S.; Brooks, J. S. *J. Appl. Phys.* **2004**, *95*, 6900−6905.
(4) Furdyna, J. K. *J. Appl. Phys.* **1988**, *64*, R29−R64.
(5) Norman, T. J., Jr.; Magana, D.; Wilson, T.; Burns, C.; Zhang, J. Z.; Cao, D.; Bridges, F. *J. Phys. Chem. B* **2003**, *107*, 6309−6317.
(6) Erwin, S. C.; Zu, L.; Haftel, M. I.; Efros, A. L.; Kennedy, T. A.; Norris, D. J. *Nature* **2005**, *436*, 91−94.
(7) Mikulec, F. V.; Kuno, M.; Bennati, M.; Hall, D. A.; Griffin, R. G.; Bawendi, M. G. *J. Am. Chem. Soc.* **2000**, *122*, 2532−2540.
(8) Feltin, N.; Levy, L.; Ingert, D.; Pileni, M. P. *J. Phys. Chem. B* **1999**, *103*, 4−10.
(9) Cumberland, S. L.; Hanif, K. M.; Javier, A.; Khitrov, G. A.; Strouse, G. F.; Woessner, S. M.; Yun, C. S. *Chem. Mater.* **2002**, *14*, 1576−1584.
(10) Hanif, K. M.; Meulenberg, R. W.; Strouse, G. F. *J. Am. Chem. Soc.* **2002**, *124*, 11495−11502.
(11) Raola, O. E.; Strouse, G. F. *Nano. Lett.* **2002**, *2*, 1443−1447.
(12) Meulenberg, R. W.; van Buuren, T.; Hanif, K. M.; Willey, T. M.; Strouse, G. F.; Terminello, L. J. *Nano Lett.* **2004**, *4*, 2277−2285.

ferromagnetic exchange between Mn ions clustered in the dimensionally confined lattice. Thermally driven clustering of Mn into larger domains in the CdSe host lattice is believed to give rise to the observed SPM phenomenon. Magnetic susceptibility, magnetization studies, and EPR measurements confirm that the magnetic effects can be explained in terms of a doubling of the Mn cluster domain content. The presence of an exchange interation ($J_{ij}\vec{S}_i\cdot\vec{S}_j$) between two magnetic spins ($\vec{S}_i,\vec{S}_j$) is evidence of the clustering of Mn(II) ions. The exchange interaction is evident in the magnetic susceptibility as a deviation from the Curie law, in which the Curie−Weiss constant is necessary to fit the beginning of the magnetic phase. The Curie temperature is proportional to the exchange interaction present in the system ($T_c = (J_{ij}s(s+1))/3k_B$),[13] where J_{ij} is the exchange energy, s is the spin of the interacting ion, and k_B is Boltzmann's constant. No evidence for loss of Mn(II) or change in nanoparticle size is observed following chemical treatment, suggesting the ion clusters exist within the nanoparticle, although the exact location within the quantum dot is not discernible.

In doped nanomaterials[10,14−16] the influence of clustering in chemically prepared systems has been speculated to influence the magnetic behavior in Co/CdSe nanoparticles at high concentrations of Co (>20%).[10] Thermally driven ion clustering in bulk materials is a known phenomenon that tailors the formation of magnetic, structural, and electronic domains.[15,17,18] Mullin and co-workers have observed ion migration effects for a series of single-crystal Mn/HgSe samples.[19] Mullin observed changes in magnetism following thermal annealing (230 °C) of samples with <1% Mn which he correlated with the change in cluster content following thermal annealing. This was also observed by Galazka[20] and Oseroff[21] where the amount of clustering was twice that predicted for the working concentration. This is also evident from the EPR and magnetic susceptibility in other systems such as Mn/CdS where the manganese interactions are evident from the dipolar (electron−electron) broadened EPR data[8,22] and a magnetic susceptibility that includes clusters was added to fit the observations.[19−21] Using clustering statistics to predict the probability of finding different sized cluster domains within the lattice, the onset of magnetism was related to the concentration of two or more localized Mn clusters in the lattice. The probability for observation of clusters in a wurtzite lattice is

$$P_1 = (1 - 12x)^{12} \quad (1a)$$

$$P_2 = 12x(1 - x)^{18} \quad (1b)$$

$$P_{3OT} = 18x^2(1 - x)^{23}(7 - 5x) \quad (1c)$$

$$P_{3CT} = 24x^2(1 - x)^{22} \quad (1d)$$

where x is the dopant molar ion concentration for a substitutional ion and three ions can be along the same plane (P_{3CT}) or different crystallographic planes (P_{3OT}).[19] This predicts, for $x = 0.01$, $P_1 = 89\%$ for isolated Mn ions, $P_2 = 10\%$ for ion pairs, and $P_3 = P_{3OT} + P_{3CT} = 1\%$ for $n = 3$ clusters statistically clustered in the lattice. From the bulk using EPR line shape arguments and susceptibility fit were shown to prove that formation of larger clusters than statistically predicted was shown by Mullin,[19] Galazka,[20] and Oseroff.[21] Within the nanocrystal lattice, each domain will have a magnetic moment and the interaction of those moments will induce a net magnetic moment for the individual nanocrystal (intradot). If the nanocrystal net magnetic moment is large enough, interdot (dipolar) coupling may lead to the observation of ferromagnetism. The observation of ferromagnetism in bulk Mn doped II−VI semiconductors requires the inclusion of interacting magnetic moments of clustered Mn centers within the lattice, and the magnetic response is dependent on the size and concentration of clusters in the lattice.[19] Due to the size constraint of the system, the observed transition is that of the single-domain characteristic transition, expected for nanosized particles. The influence of interdot coupling will not be observed in a bulk system where the cluster interactions are already inclusive and are considered domain interactions.

In nanoparticles, since the same probability for clustering of the ions exists as that for systems, annealing should induce enhanced ferromagnetic exchange by inducing cluster formation. The clustering is a result of the strain relief when there are vacancies which can raise the energy potential of its environment totaling in an electron trap. The vacancies are evident from fluorescence spectra of small nanoparticles where trap state emission is the dominant form of photoluminescence.[23] The nature of the migration is dependent on the reaction rates of formation, the nature of the defect ion, and the host lattice.[24,25]In addition, the high surface area and high strain of the nanoparticle system may influence the nature of doping and may enhance clustering to relieve strain and thus be critical in understanding the magnetic response.[2]

Experimental Section

The synthesis of the 1% doped 4.0 nm Mn/CdSe was carried out by reaction of $Li_4[Cd_{10}Se_4(SC_6H_5)_{16}]$ (Cd_{10}) and $MnCl_2$ in hexadecylamine analogous to earlier studies.[5,9−12] The reaction was carried out at 120 °C to allow Mn ion exchange with the Cd ions in the Cd_{10} cluster. Exchange of metal ions into the clusters has been observed previously.[26] Growth of the nanoparticle was conducted at 230 °C for 3 h, and isolation of a 4 nm particle was achieved by precipitation of the nanoparticle from a toluene solution through the addition of MeOH. The product was cleaned 3 times using toluene/methanol, followed by three sequential pyridine ligand exchanges at 70 °C in order to remove unincorporated Mn ions. For the experimental studies, the isolated sample was divided into two parts, a preannealed and a postannealed sample. The postannealed sample was generated by dissolution of the

(13) Ashcroft, N. W.; Mermin, N. D. *Solid State Physics*; Thomson Learning, Inc.: Toronto, 1976.
(14) Norris, D. J.; Yao, N.; Charnock, F. T.; Kennedy, T. A. *Nano Lett.* **2001**, *1*, 3−7.
(15) Norberg, N. S.; Kittilstved, K. R.; Amonette, J. E.; Kukkadapu, R. K.; Schwartz, D. A.; Gamelin, D. R. *J. Am. Chem. Soc.* **2004**, *126*, 9387−9398.
(16) Chen, W.; Joly, A. G.; Zhang, J. Z. *Phys. Rev. B* **2001**, *64*, 041202.
(17) Nagata, S.; Galazka, R. R.; Mullin, D. P.; Akbarzadeh, H.; Khattak, G. D.; Furdyna, J. K.; Keesom, P. H. *Phys. Rev. B* **1980**, *22*, 3331−3343.
(18) Hsu, K. F.; Loo, S.; Guo, F.; Chen, W.; Dyck, J. S.; Uher, C.; Hogan, T.; Polychroniadis, E. K.; Kanatzidis, M. G. *Science* **2004**, *303*, 818−821.
(19) Mullin, D. P. Microwave Studies of Semimagnetic Semiconductors. Thesis, Purdue University, 1980.
(20) Galazka, R. R.; Nagata, S.; Keesom, P. H. *Phys. Rev. B* **1980**, *22*, 3344−3355.
(21) Oseroff, S. B. *Phys. Rev. B* **1982**, *25*, 6584−6594.
(22) Lu, J.; Wei, S.; Yu, W. C.; Zhang, H. B.; Qian, Y. T. *Chem. Mater.* **2005**, *17*, 1698−1703.
(23) Miyake, M.; Torimoto, T.; Nishizawa, M.; Sakata, T.; Mori, H.; Yoneyama, H. *Langmuir* **1999**, *15*, 2714−2718.
(24) Friauf, R. J. *J. Appl. Phys.* **1962**, *33*, 494.
(25) Mapother, D.; Crooks, H. N.; Maurer, R. *J. Chem. Phys.* **1950**, *18*, 1231.
(26) Lover, T.; Henderson, W.; Bowmaker, G. A.; Seakins, J. M.; Cooney, R. P. *Inorg. Chem.* **1997**, *36*, 3711−3723.

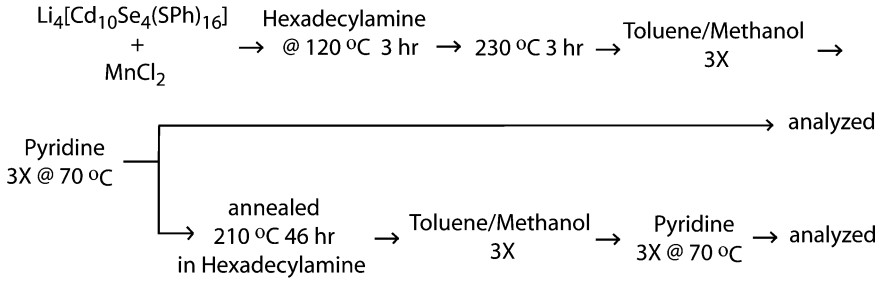

Figure 1. Flowchart of the synthesis and annealing procedure.

Table 1. Size Comparison in Pre- and Postannealed Nanoparticles Using Scherrer Broadening and TEM Measurement

preannealed		postannealed	
2θ ⟨*hkl*⟩	size (Å)	2θ ⟨*hkl*⟩	size (Å)
41.91	48.7	42.05	48.48
45.51	43.88	45.65	42.81
49.33	44.93	49.54	45.46
TEM size	39	TEM size	39

Table 2. Wurtzite Lattice Constants of CdSe and Pre- and Postannealed Mn/CdSe

	a (Å)	*c* (Å)	*c*/*a*
CdSe	4.299	7.011	1.631
Mn/CdSe preannealing	4.310	7.071	1.641
Mn/CdSe postannealing	4.296	7.051	1.641

pyridine capped Mn/CdSe sample in hexadecylamine at 210 °C for 46 h and isolation as described above (Figure 1).

Discussion

UV−visible, powder X-ray diffraction, and TEM were obtained for the pre- and postannealed sample to verify no significant change in particle diameter or structure occurs. The first exciton in the absorption spectroscopy for the preannealed sample is at 2.30 eV corresponding to a 3.7 nm nanoparticle and is found to shift 21 meV to lower energy following annealing, suggesting growth by approximately a single lattice plane (3.8 nm). Size distribution for these samples is 10% based on the fwhm of the first excitonic feature. Powder XRD identifies a wurtzite crystal structure for both the pre- and postannealed sample with an average size of 4.6 nm based on a Scherrer broadening analysis of the ⟨110⟩, ⟨103⟩, and ⟨112⟩ reflections (Table 1). The PXRD (4.6 nm), absorption (3.7 nm), and TEM (3.9 nm) are in reasonable agreement, with the larger value from PXRD suggesting the materials are highly crystalline.

The shifts in the pXRD lattice constants relative to a 4 nm CdSe sample isolated identically to the Mn/CdSe samples are summarized in Table 2. The pXRD reflections exhibit a compression between the pre- and postannealed samples of 0.014 Å, which is larger than the expected 0.0012 Å for a 1% Mn(II) doping on the Cd(II) site. While pXRD can provide evidence of doping, the observation can be skewed by internal clustering within the lattice leading to a nonlinear deviation. Thermal ion migration of the Mn ions in the wurtzite CdSe quantum dot into small cluster domains is expected to relieve strain induced by the ∼16% lattice contraction about the Mn ion. The larger observed compression in the pXRD data suggests clustering may be present in these materials and larger than theoretically predicted. Following annealing the increased compression may suggest increased clustering by ion migration is occurring.

Enhanced clustering in these materials following annealing is further evident upon inspection of the magnetic data. The magnetic behaviors of the pre- and postannealed samples in solution and as powders are dramatically different (Figure 2). For the postannealed powder sample, the magnetic susceptibility under zero field cooled, and field cooling at 100, 200, 400, and 600 G is shown (Figure 2A). Figure 2D shows the magnetic susceptibility of the powdered postannealed sample at 100 G field cooled with a Brillouin function fit to the high-temperature portion of the data. The data for the preannealed sample at zero field cooled (ZFC) to fit a Brillouin function over the complete temperature range is shown in Figure 2C. Field cooling of the preannealed sample does not influence the magnetic data.

In the preannealed sample the solution and powder data are those of a classical paramagnet. The data for the postannealed sample at zero field exhibit a peak at 11 K, while the powdered preannealed sample lacks such a peak. In the solution data for the postannealed sample (Figure 2B), the feature is shifted to lower temperature, occurring at 4 K. Inspection of the temperature-dependent deviation of the magnetic susceptibility trace observed at 100 G compared to ZFC for the powdered postannealed sample suggests that the sample has a blocking temperature (T_B) of 40 K (Figure 2A). Alternatively, the 40 K transition may be due to spin glass behavior. ac-susceptibility measurements, as detailed below, suggest this is not a classic spin glass. The observation of the magnetic feature 30 K below T_B can be attributed to a distribution in exchange energies for different sized clusters within the nanoparticles or nanoparticle−nanoparticle interactions (interdot). This means that the moments of the individual clusters within a given nanocrystal will freeze at different temperatures, and only the average freezing point of the ensemble of intradot and interdot interactions will appear as a feature in the susceptibility curves. Consistent with this observation the 11 K feature is observable even at 100 G. The low-temperature transition is due to the interdot interactions of superexchange between the Mn ions.

One possible method to analyze the interdot contributions to this feature is dilution experiments. Upon dilution the 11K feature disappears in the susceptibility traces (Figure 2). The loss of the 11 K feature upon dilution of the postannealed sample into octylamine (Figure 2B) may be due to loss of intraparticle magnetic exchange; however a more likely cause is a change in the interparticle interactions, while the solvent causes a large diamagnetic background that inhibits the ability to see any evidence of the higher transition. Interdot coupling effects have been observed to contribute the magnetic susceptibility by Rotello,[27] with a change in the blocking temperature upon

(27) Frankamp, B. L.; Boal, A. K.; Tuominen, M. T.; Rotello, V. M. *J. Am. Chem. Soc.* **2005**, *127*, 9731.

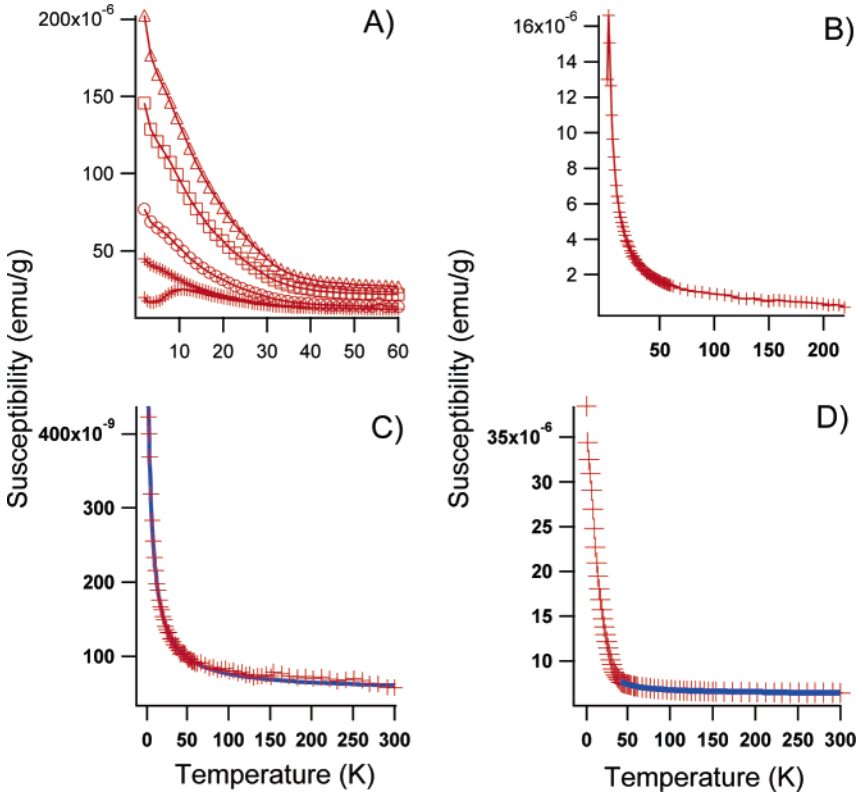

Figure 2. Magnetic susceptibility of pre- and postannealed 1% Mn/CdSe. (A) Postannealed zero field cooled (bottom curve) and field cooled at 100 (+), 200 (○), 400 (□), and 600 G (△). (B) Postannealed field-cooled in Trioctylamine. (C) Preannealed field-cooled. (D) Postannealed field-cooled with a Brillouin function fit.

dilution of Fe_2O_3. The results of the dilution experiment are suggestive of interparticle interactions in the Mn/CdSe system. This is probable if the individual magnetic moments of the clusters within the dot couple to give rise to a large magnetic moment for the single-domain-like nanocrystal.

The powder samples show high-temperature paramagnetism with differences in the contribution of exchange following annealing. This can be analyzed by fitting the temperature-dependent magnetic susceptibility data for the powder samples to a Langevin (eq 2a) and Brillouin function (eq 2b).[13]

$$\chi = \frac{N_0 g \mu_B J B_j(\eta)}{H} \tag{2a}$$

$$B_j(\eta) = \frac{2J+1}{2J}\coth\left(\frac{2J+1}{2J}\eta\right) - \frac{1}{2J}\coth\left(\frac{1}{2J}\eta\right) \tag{2b}$$

$$\eta = \frac{gJH}{k_B(T-\theta)} \tag{2c}$$

Equation 2a is fit by allowing the values for N_0, J, and θ to float and the best fit parameters analyzed by nonlinear regression. Prior to fitting the magnetic susceptibility data, the diamagnetic contribution from the host lattice is subtracted using the measured susceptibility on a 4 nm CdSe sample treated identically to the Mn/CdSe samples. In the equations, N_0 is the molar volume, g is the Landé g-factor, μ_B is the Bohr magneton, J is the spin, and H is the applied magnetic field. The g value used (2.004) is obtained from EPR, as described below. To fit the susceptibility, the Brillouin function (eq 2b) is used with η (eq 2c) being equal to the ratio between the spin components and the thermal energy, where k_B is Boltzmann's constant and θ is the experimental Curie temperature.

The preannealed sample can be fit over all temperature ranges as a paramagnet. The postannealed sample can only be fit at high temperature to the Brillouin function due to increased exchange interactions below 40 K. For the pre- and postannealed sample a value of $J = {}^5/_2$ is measured using the Curie−Weiss equations (eq 2) as expected for Mn(II). The Curie temperatures calculated for the pre- (−0.23 K) and postannealed (20 K) sample are dramatically different indicating a switch from AFM to FM exchange following annealing. At low concentrations this is expected from the observations gathered from Oseroff.[21] The larger Curie temperature for the postannealed sample is due to increased Mn ion clustering in the quantum dot lattice. In this size regime, the onset of ferromagnetic exchange should lead to SPM, which is confirmed by frequency dependent experiments on the postannealed sample between 8 and 850 Hz (Figure 3). As seen in the ac-magnetic susceptibility, the largest tangential loss occurs for the data collection at 8 Hz at 10 K with no detectable loss at 40 K.

The lack of a detectable transition at 40 K in Figure 3 does not indicate spin-glass behavior, but rather a slow magnetization occurs in these materials with formation of an SPM based on the ac results. Assignment of SPM rather than spin glass in this sample is obtained by using the criterion introduced by Mydosh, where the value of $\varphi = \Delta T/T_f\Delta(\log \omega)$.[28]

For a spin glass the value is typically on the order of 10^{-2}, while for an SPM the φ range is 10^{-1}−10^{-2}.[28] Using this convention, the postannealed sample exhibits a value of 0.16 consistent with the individual quantum dots being SPM. EPR can provide evidence of the degree of Mn clustering, as well as

(28) Culp, J. T.; Park, J. H.; Meisel, M. W.; Talham, D. R. *Inorg. Chem.* **2003**, *42*, 2842−2848.

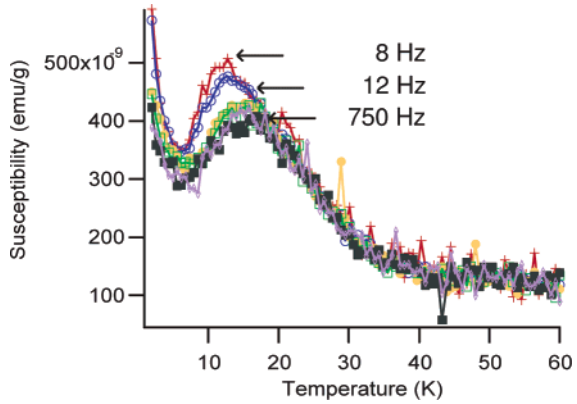

Figure 3. Magnetic (ac) susceptibility of postannealed Mn/CdSe with a 4 Oe oscillating field at (+) 8 Hz, (○) 12 Hz, (●) 250 Hz, (□) 350 Hz, (■) 750 Hz, and (◇) 850 Hz.

discrete information of the Mn doping site, and the Mn oxidation state. Mn(II) clustering will lead to dipolar broadening with loss of hyperfine structure. Q-band EPR measurements were performed at room temperature on powdered Mn/CdSe samples (Figure 4). For Mn(III), an $s = 2$ Jahn−Teller ion is not observed in the EPR data for either sample and would give an EPR signature at a lower field (higher g-value) if present with a much wider line width due to zero-field splitting. Assignment of the two contributions to the EPR spectra is gained by inspection of Q-band and X-band data, as well as power dependent measurements.[29]

There are two observable contributions to the EPR spectra, an exchange broadened (clustered Mn) term and a hyperfine split (isolated sites) term. The g-value for both samples are identical within experimental error ($g = 2.004$). The calculated g value is well within the literature range 2.001−2.006 for Mn(II) doped II−VI semiconductors.[30]

The EPR data (Figure 4) for the pre- and postannealed samples are similar at room temperature with a strong hyperfine feature (six-line pattern) for Mn(II) and a broad dipolar term. The dipolar term is increased in relative magnitude in the postannealed sample. Lowering the temperature facilitates the observation of the broad dipolar component in both samples which is correlated to the onset of magnetic exchange observed in Figure 2. At 5 K the difference is more dramatic with preannealed sample being composed primarily of isolated manganese with a small dipolar contribution, while the postannealed sample contains less than a percent of isolated manganese and is dominated by the dipolar term. The larger ferromagnetic exchange constant in the postannealed sample observed in the temperature-dependent magnetization plots suggests the dipolar term should saturate at low T. In the postannealed sample saturation of the dipolar signal is observed below the blocking temperature (Figure 3D).

Analysis of the hyperfine structure in Figure 3 provides insight into the site occupation of the Mn. The smaller Mn ion is expected to distort in the CdSe lattice, which is observable in the EPR data (Figure 4). The EPR data suggest the Mn site is a trigonally or tetragonally distorted T_d which leads to the observation of forbidden EPR transitions attributed to a stronger spin−orbit term arising from symmetry breaking and is assigned to the $-1/2 \rightarrow 1/2$.[31] Van Wierengen demonstrated the magnitude of the Mn^{2+} hyperfine splitting constant is dependent on the covalency of the site occupied by the manganese ion with more ionic sites exhibiting larger hyperfine constants. This empirical observation allows insight into the location of the manganese to be gained with respect to the different possible sites present in a nanoparticle (core or surface). One expects the surface sites to be more ionic than the more bulklike core, and therefore surface Mn ions should exhibit a larger hyperfine splitting than internal Mn ions. Consistent with this assumption, values for the hyperfine constant of $62-65 \times 10^{-4}$ cm^{-1} are observed for internal Mn ions in bulk Mn/CdSe,[30] and larger hyperfine splittings (85×10^{-4} cm^{-1}) were observed for Mn ions isolated on the surface of CdSe.[7] The measured hyperfine splitting constant in both the pre- and postannealed sample is 62.0×10^{-4} cm^{-1}. This allows assignment of core doping of the Mn into the CdSe in these materials.

Perhaps the most significant observation in the EPR is the ratio of the two EPR absorptions in both samples. Inspection of the ratio of the EPR signatures indicates the dipolar term for both samples contributes ∼80−90% of the EPR signature, inconsistent with a statistical doping value of 1% predicted by the probability functions in eq 1. By integrating the EPR signals, the hyperfine term accounts for 24% of the signal in the preannealed sample but only about half (12%) in the postannealed sample. The drop in the hyperfine component following annealing correlates with the observed onset of ferromagnetism in the postannealed sample. This result supports the earlier assumption of thermal annealing leading to increased Mn ion clustering in the CdSe quantum dot and to the onset of ferromagnetic exchange following annealing. The observation of intradot and interdot interactions contributing to the onset of SPM behavior in the postannealed sample can be verified by inspection of the field dependent magnetization plots in Figure 5. Following annealing, a coercive field of 95 mT (Figure 5A and Figure 6A) with magnetic saturation at 2 T ($M_{sat} = 3600$ emu/mol of Mn) is observed at 2 K (Figure 5A). The preannealed sample at 2 K shows no field dependent magnetization and can be fit to a purely paramagnetic exchange interaction consistent with a low concentration of Mn clusters being present in the preannealed sample. In solution no observable coercivity is evident at any temperature (Figure 5B and D) due to the large diamagnetic contributions to the signal and loss of interdot interactions. In the postannealed powdered sample the coercivity is reduced as the temperature increases with a coercivity of 0.006 T at 20 K (Figure 5C) and a loss of saturation above the blocking temperature (Figure 6B) due to thermalization of the spins. Surprisingly, above 20 K the coercivity (0.001 T) saturates and remains constant up to 250 K (Figure 6C). This is a surprising result, and it is not well understood at this time why the ferromagnetism continues as far as it does. Experimentally, while this may be conveniently explained away as an artifact, we observed no magnetization in undoped samples in this region and no magnetization from the capsule, and the weak coercivity is observable on more than one SQUID indicating that it is not instrument specific and may be real. A likely possibility is the high-temperature magnetization may arise from larger domain structures of Mn−Se−Mn and quite possibly

(29) Magana, D.; Strouse, G. In preparation.
(30) Van Wieringen, J. S. *Discussions of the Faraday Society* **1955**, *19*, 118.
(31) Igarashi, T.; Ihara, M.; Kusunoki, T.; Ohno, K.; Isobe, T.; Senna, M. *J. Nanopart. Res.* **2001**, *3*, 51−56.

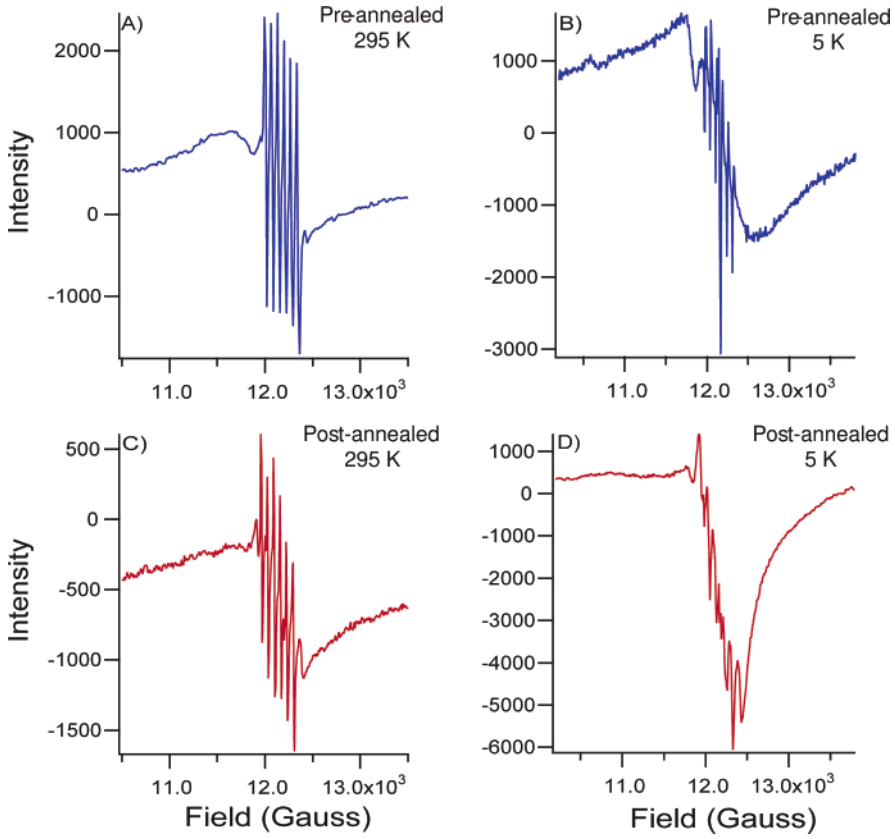

Figure 4. Room temperature and 5 K Q-band EPR of pre- and postannealed Mn/CdSe. (A) Preannealed at room temperature. (B) Preannealed at 5 K. (C) Postannealed at room temperature. (D) Postannealed at 5 K.

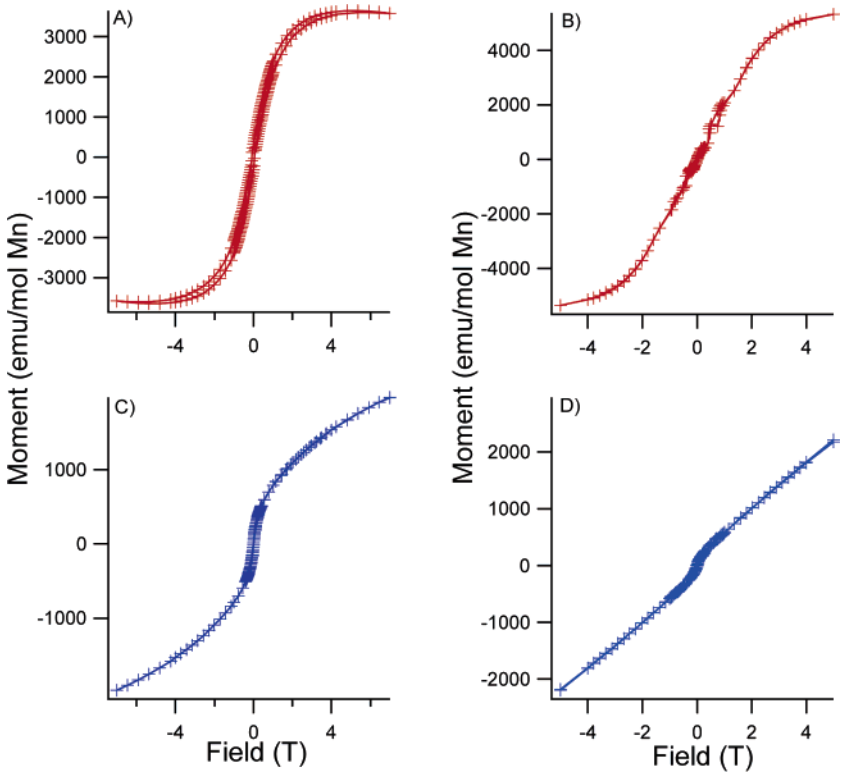

Figure 5. Magnetization of the postannealed Mn/CdSe sample at (A) 2 K as powder, (B) 2 K in Trioctylamine, (C) 20 K as powder, (D) 20 K in Trioctylamine.

interdot coupling of remnant magnetic moments in the nanocrystalline sample. Further studies are underway to prove or disprove this observation.

The saturation at 20 K rather than at the blocking temperature implies two competing interactions determine the observed magnetic behavior. The observation of high-temperature coer-

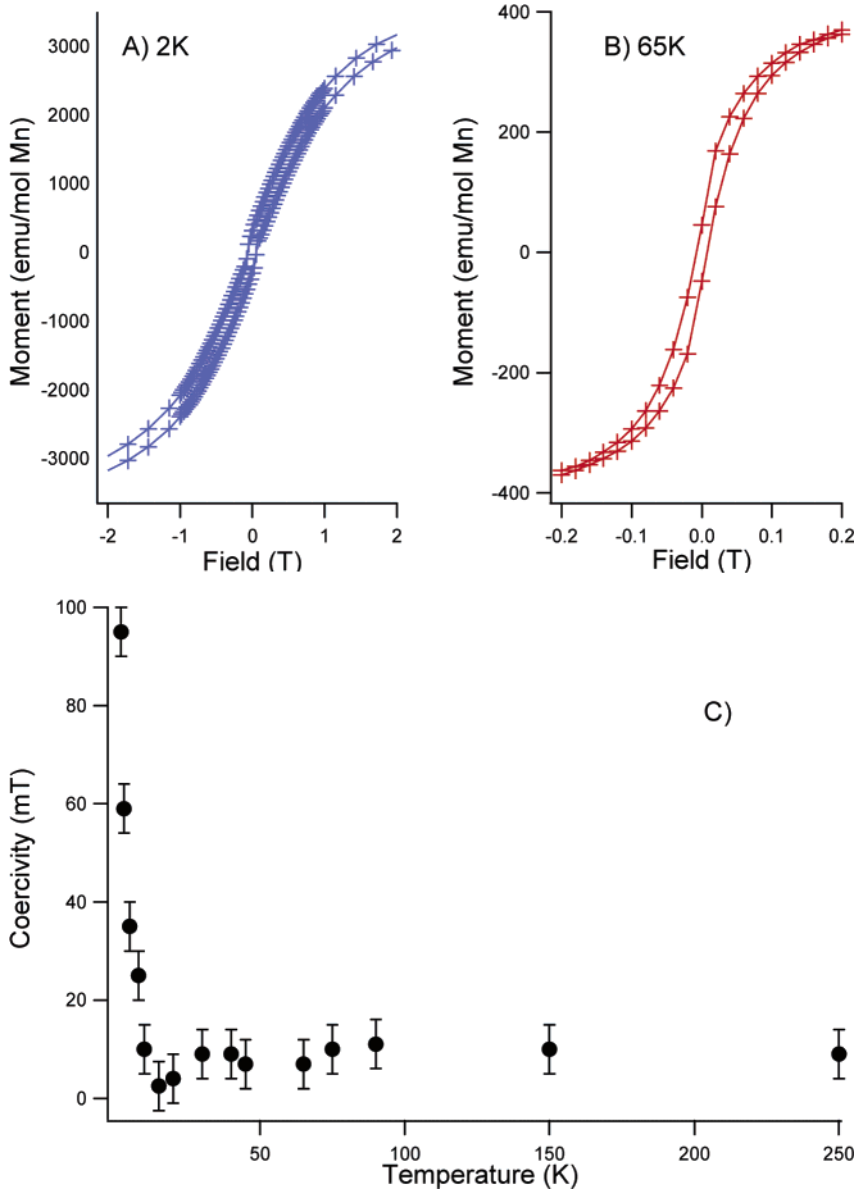

Figure 6. Magnetization of the postannealed Mn/CdSe sample at (A) 2 K and (B) 65 K. (C) Plot of the coercive field as a function of temperature.

civity suggests the second ferromagnetic interaction persists to temperatures above 250 K, while the SPM phase has diminishing contributions to the total magnetic behavior as the blocking temperature 40 K is approached. The surprising observation of the high temperature ferromagnetism is speculated to arise from particle−particle interactions due to particle aggregation at the nanoparticle unpassivated facets. To verify that this second magnetization feature arises from the material rather than the cavity, the magnetization of the preannealed sample and nondoped CdSe was measured and no magnetization transition was observed for these samples. In addition, the SQUID response was checked with an empty capsule to make sure that the signal was not from the magnet hysteresis. Evidence of the second magnetic transition in the postannealed sample is apparent in the field dependent magnetization plots between 2 and 65 K (Figure 7).

The observed behavior as a function of temperature requires fitting to the superposition of two separate magnetization functions, whose contribution varies independently with temperature. Although the fit to a superposition of two ferromagnetic transitions is not entirely correct since the Brillouin magnetization function requires no spin interactions to be present, it is still empirically useful in interpreting the presence of the secondary magnetic dipolar interaction.

At 2 and 5 K, the field dependent data are dominated by the low temperature magnetization term and can be approximately fit to a single magnetization event using the Brillouin function, $M(H) = N\mu_0 gJB_J(gH\mu_0/2k_BT)$, where N is the molar volume, μ_0 is the Bohr magneton, g is the free electron Landé g-value, and J is the spin. Fitting of the magnetization Brillouin function indicates the spins at 2 and 5 K are higher than expected with values of $J_{2K} = 2.7$ and $J_{5K} = 3.0$. As the temperature is increased, the magnetic data require a superposition of the two species, with the first component becoming paramagnetic above the blocking temperature. At 65 K, the magnetic data are cleanly fit to two contributions with the second term exhibiting magnetization saturation at lower field, ∼0.2 T, and a small value for magnetization saturation (3 emu/mol of Mn). The

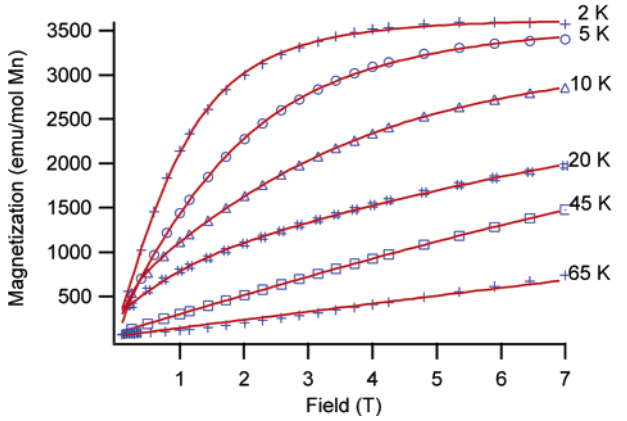

Figure 7. Magnetization of the postannealed Mn/CdSe at 2, 5, 10, 20, 45, and 65 K where the fit is represented by the solid line.

secondary (high temperature) magnetization is believed to be dominated by interdot coupling due to remnant magnetization moments of the internal clusters producing a net dot moment, while the low T magnetization event reflects the onset of a single-domain SPM phase in the total ensemble of nanocrystals (Figure 8). Evidence of a long-range interdot coupling process is gained by analyzing the spin (J) of the susceptibility data using the magnetization Brillouin function. The first magnetic contribution was calculated to have a value of $J_1 = 3.8$ ($N_1 =$ 99.4% molar contribution) and the second term $J_2 = 110$ (N_2 $= 0.6\%$ molar contribution) at all temperatures. The high spin value for the second species implies that this cannot be accounted for by simply assuming large magnetic clusters being present in the lattice. The small total contribution to the magnetic moment of the second magnetization event indicates that this is most likely due to interdot coupling as suggested above, rather than an intradot magnetic transition. This is supported by the dilution experiments in Figure 1. The onset of the SPM behavior in these materials arises from sample annealing, which induces the Mn ions to migrate within the lattice and begin to form $n >$ 2 ion clusters. (Figure 8a) The Mn−Mn−Mn interactions give rise to a magnetic moment that form single-domain-like quantum dots in the powdered ensemble. While ion-migration processes in CdSe bulk are small (10^{-2} m^2/s) for hexagonal lattices, the observation of annealing effects in these materials suggests the Mn ions have enhanced diffusion rates or the ion diffusion may occur along vacancies present in the growing particle to relieve strain. The change in magnetic behavior following annealing allows a model to be developed that explains the magnetization and EPR results. The SPM phase below 40 K is due to both intra- and interdot coupling events arising from freezing of the spin of the clusters within a given nanocrystal. This results in a large magnetic moment producing the single-domain-like quantum dot that can then couple the ensemble of dots producing a coercive field (Figures 6 and 8b). Above 40 K, the nearly constant coercivity is assigned to interdot interactions arising from the remnant weak magnetic moments of the larger clusters within the quantum dot (Figure 8c) occurring between aggregated nanoparticles . The interdot magnetization is expected for pyridine passivated nanocrystalline samples due to their propensity for agglomeration into larger superlattices when precipitated from solution. It is known that the agglomeration for CdSe materials has a high likelihood of forming with conservation of crystallographic faces, which would enhance

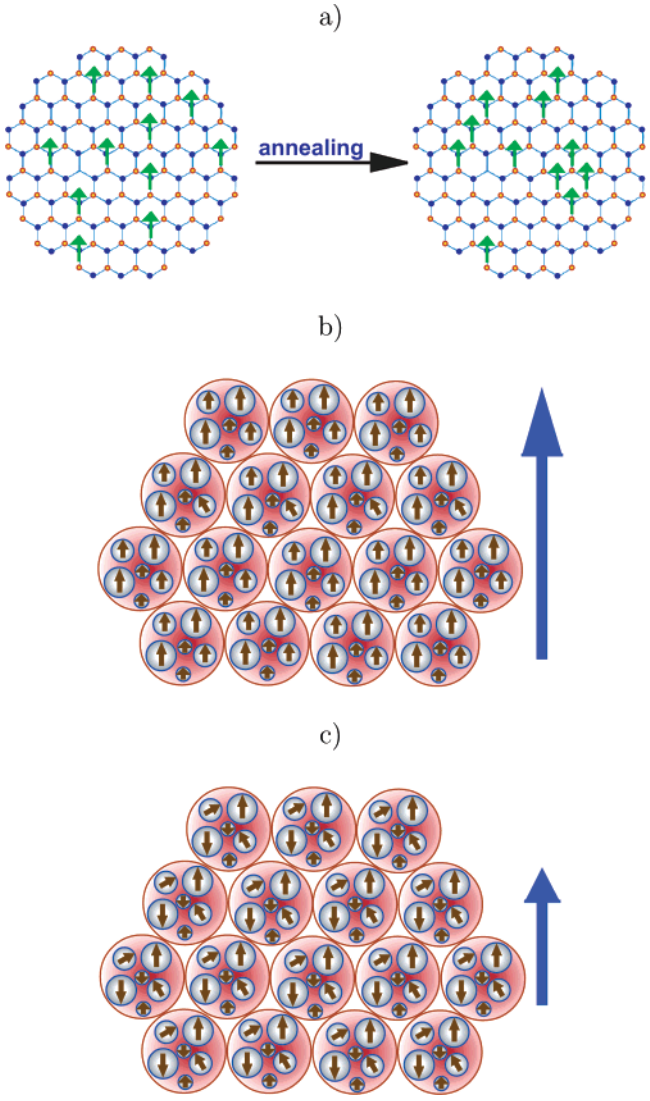

Figure 8. (a) Intradot interactions of the Mn spins in a hexagonal (wurtzite) lattice where the cadmium, selenium, and manganese atoms are represented by dots that are blue, red, and green, respectively. Upon annealing the Mn(II) ions tend to cluster giving rise to ferromagnetic interactions leading to a larger magnetic moment. (b) Magnetization below 40 K with the slow onset of the superparamagnetic phase with formation of single-domain quantum dots. (c) Magnetization above 40 K arising from weak interdot interactions of remnant spin on larger clusters within the individual quantum dot.

the probability of these interactions.[32] Similar observations of interdot coupling have been suggested to account for the observed magnetic anomalies in superparamagnet Fe_2O_3 nanoparticles isolated as powders from solution.[27]

Conclusion

Thermal annealing with formation of paramagnetic ion domains provides a mechanism to manipulate ferromagnetic exchange in semimagnetic quantum dot systems. The magnitude of the exchange interaction between the Mn^{2+} ions in Mn/CdSe quantum dots is dictated by the position and number of Mn in the cluster and accounts for the observed magnetization for the Mn/CdSe samples studied. The assignment of the 40 K blocking temperature rather than at the observed anomaly at 11 K is

(32) Murray, C. B.; Kagan, C. R.; Bawendi, M. G. *Annu. Rev. Mater. Sci.* **2000**, *30*, 545−610.

accounted for by the distribution of cluster sizes and separation distances for the clusters within an individual quantum dot. The temperature-dependent EPR spectrum, which is a convenient probe for measuring the magnitude of clustering in these materials, exhibits an increase in the broad component below the blocking temperature suggesting that this term is coupled to the ferromagnetic onset in the postannealed Mn/CdSe sample in line with the proposed model. In conclusion, this study demonstrates that enhancing clustering in the lattice by thermal annealing can switch on ferromagnetism in doped semiconductors, pointing to an intriguing method to tailor the magnetic properties in quantum dot semimagnetic systems.

Acknowledgment. We wish to acknowledge NSF-CAREER (DMR-9875940) for financial support.

JA055785T